Reverse energy pooling in a K-Na mixture

G. De Filippo, S. Guldberg-Kjær, S. Milošević,* and J. O. P. Pedersen
Niels Bohr Institute, Ørsted Laboratory, Universitetsparken 5, DK-2100 Copenhagen Ø, Denmark

M. Allegrini
Istituto Nazionale per la Fisica della Materia, Dipartimento di Fisica, Università di Pisa, Piazza Torricelli 2, I-56126, Pisa, Italy and Dipartimento di Fisica della Materia e Tecnologie Fisiche Avanzate, Università di Messina, Salita Sperone 31, I-98166, Sant'Agata-Messina, Italy

(Received 19 June 1997)

We report experimental rate coefficients for the reverse heteronuclear energy-pooling collisions $K(5D)+Na(3S)\rightarrow K(4P)+Na(3P)$ and $K(7S)+Na(3S)\rightarrow K(4P)+Na(3P)$ at thermal energies. Both reactions are exothermic and very high rates were observed showing that reverse exothermic energy-pooling is an order of magnitude more efficient than the corresponding forward endothermic energy-pooling reactions. This is in accordance with the general behavior of the exothermic and endothermic energy-pooling rate coefficients in alkali-metal atoms. In the experiment the potassium atoms were excited in two steps to either the $5D$ or $7S$ state via the $4P$ level using two broadband cw dye lasers. A double-modulation technique has been used to select the fluorescence contributions at the $Na(3P_J)$ exit channels due only to the above reactions. The ground-state sodium and potassium atom densities were measured by the absorption of lines from a K-Na hollow-cathode lamp. The measured densities and fluorescence intensities have been used to obtain absolute reverse energy-pooling rate coefficients. The contribution to the rate coefficients from other processes are discussed. [S1050-2947(98)03901-8]

PACS number(s): 34.90.+q, 34.50.Rk

I. INTRODUCTION

Collision processes where electronic excitation energy is transferred have been studied both theoretically and experimentally for decades. A particularly interesting process is energy pooling where two excited atoms collide and produce one highly excited atom and one ground-state atom [1]. In the experimental studies the colliding atoms are typically prepared in the excited state using optical excitation, and the highly excited atoms, populated by the energy-pooling collisions, are detected through their fluorescence.

The first reported study of heteronuclear energy pooling (EP) was performed by Allegrini *et al.* [2] in a mixed vapor of potassium and sodium upon irradiation by two cw dye lasers tuned to the D resonance lines of sodium and potassium. In a later study [3] the collision cross section for the processes

$$K(4P)+Na(3P)\rightarrow K(4S)+Na(3D), \tag{1}$$

$$K(4P)+Na(3P)\rightarrow K(5D,7S)+Na(3S) \tag{2}$$

were measured relatively to the homonuclear EP process $Na(3P)+Na(3P)\rightarrow Na(3S)+Na(5S)$. The fluorescence from the high-lying levels of potassium and sodium was analyzed using an intermodulation technique to isolate the contribution due only to the heteronuclear processes.

Including the results from a following work on the K-Rb and Na-Rb systems, together with existing data for homonuclear cases, an empirical rule was obtained [4] for the dependance of EP rate coefficients on the energy defect of the collision in the case of the exothermic channels. It was found (see Fig. 3 of Ref. [4]) that the magnitude of the rate coefficient k at a temperature T depends on the value of the energy defect ΔE according to the exponential decay function

$$k=A\ \exp\left[-\left(\frac{\Delta E}{k_B T}\right)^B\right], \tag{3}$$

where $A=(5.5\pm 1.7)\times 10^{-9}\ \mathrm{cm^3\ s^{-1}}$, $B=1.4\pm 0.2$, and k_B is the Boltzmann constant. For endothermic processes the rate coefficients were generally an order of magnitude smaller than the exothermic processes, but also a larger spread was observed not allowing the derivation of any rule. For certain endothermic EP processes this pointed towards the need to study their exothermic counterpart, the reverse energy pooling (REP) in which an atom prepared in a highly excited state collides with an atom in the ground state, and the result of the collision are two excited atoms. In addition, the large cross sections expected for REP processes are foreseen as crucial to initiate large populations of excited alkali atoms relevant for different ionization mechanisms in a dense alkali vapor [5,6] or a laser-guided discharge [7]. Such a REP process was observed by Yabuzaki *et al.* [8] in cesium vapor $[Cs(6D)+Cs(6S)\rightarrow Cs(6P)+Cs(6P)]$, preparing the initial state as a result of a stepwise laser excitation via the Cs_2 dimer. They found a cross section of $(1.5^{+1.5}_{-0.7})\times 10^{-14}\ \mathrm{cm^2}$ at 530 K. The cross sections for the forward EP process $Cs(6P)+Cs(6P)\rightarrow Cs(6D)+Cs(6S)$ have recently been obtained selectively with $6P_{1/2}+6P_{1/2}$ and $6P_{3/2}+6P_{3/2}$ as the entrance channels [9]. Direct comparison of

*Permanent address: Institute of Physics, P.O. Box 304, HR-10000 Zagreb, Croatia.

REP and EP cross sections in this case is complicated due to the fact that the processes are endothermic or exothermic depending on the different J combinations.

For experiments dealing only with atomic levels, the identification of REP by fluorescence detection is complicated in a homonuclear system, since the lower states can be populated both by the REP process and by radiative decay of the optically excited atom in the entrance channel. A heteronuclear system, on the contrary, offers the advantage that fluorescence from the atomic species not directly prepared by the laser excitation can be detected. Recent calculations of relevant potential-energy curves of the K-Na system [10] facilitate the selection of that particular system as a REP test case. We also believe that our methodological approach to the study of REP collisions in heteronuclear systems has a promising application as a powerful diagnostic of excited-state collision complexes. In addition, the investigated process is experimentally analogous to measurements trying to control photochemical reaction paths, where several schemes have been proposed using the interference between two continuous-wave or pulsed lasers [11]. Very recently control over the product branching ratio in photodissociation of Na_2 into $Na(3S)+Na(3P)$ and $Na(3S)+Na(3D)$ was demonstrated using a two-photon incoherent interference control scenario [12].

It is the purpose of this paper to present quantitative experimental results for rate coefficients and cross sections for the reverse K-Na energy-pooling process of Eq. (2):

$$K(5D)+Na(3S)\rightarrow K(4P)+Na(3P), \tag{4}$$

$$K(7S)+Na(3S)\rightarrow K(4P)+Na(3P). \tag{5}$$

Preliminary experimental and theoretical results on the process $K(5D)+Na(3S)\rightarrow K(4P)+Na(3P)$ have recently been presented [13]. In this paper we extend the previous measurements with data on process (5), which allows us to compare the results of REP with two different entrance channels. In addition we give the full analytical treatment of the calculations of the rate equations, which were only briefly presented in [13]. Since the extraction of the rate coefficients is simpler for process (5) than for process (4), we only give a detailed analysis of process (4) with initial $K(5D)$ excitation.

Contrary to EP measurements where both the density and the spatial distribution of excited atoms are needed, in REP measurements one needs to know only the ground-state atom density and the relevant fluorescence ratios. Thus it is interesting to note that the study of REP makes the atom distributions in the cell less important, eliminating one of the main sources of uncertainty present in the EP measurements. In forward EP it is necessary to know the spatial distribution of the laser excited atoms because the ratio

$$\frac{\int n_{nP}(\vec{r})d^3r}{\int[n_{nP}(\vec{r})]^2d^3r} \tag{6}$$

enters into the results of the rate coefficients [where $n_{nP}(\vec{r})$ is the distribution of laser excited atoms; see, e.g., Eq. (6) in Ref. [9]). In the REP measurement, for example, for the excitation of $K(7S)$, the above ratio will be replaced by

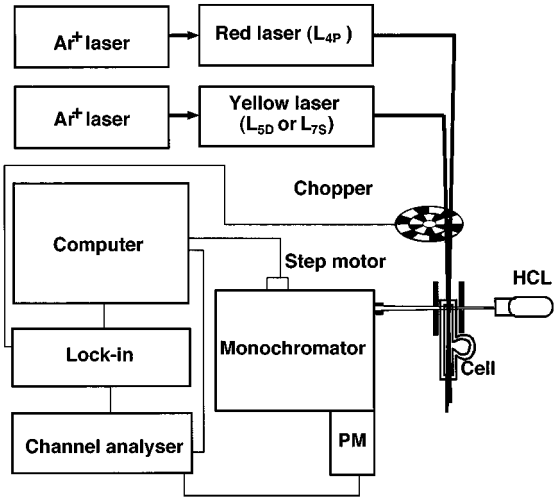

FIG. 1. Experimental setup. HCL is the hollow-cathode lamp and PM the photomultiplier.

$$\frac{\int n_{K(7S)}(\vec{r})d^3r}{\int n_{K(7S)}(\vec{r})n_{Na(3S)}(\vec{r})d^3r} \tag{7}$$

and since $n_{Na(3S)}(\vec{r})$ is uniform and thus independent of $\vec{r}$, the ratio reduces to $1/n_{Na(3S)}$.

Another advantage of the REP measurements is that the rate coefficients (to a very good approximation) are not influenced by radiation trapping effects, because as outlined in Ref. [13], the expressions for the REP rate coefficients do not depend on the radiative decay rate of highly trapped transitions. This point will be further clarified in Sec. III, and in [14] it is demonstrated that radiation trapping does not influence the radiative rates appearing in the expressions for the REP rate coefficients in the special case of cw excitation in a capillary cell.

A complication exists because starting with a high-lying excited level in the entrance channel also triggers processes other than REP, the contribution of which has to be evaluated. In this work we use two broadband cw dye lasers to excite $K(5D)$ or $K(7S)$ levels, modulate them at two different frequencies, and record the relevant fluorescence signals at the sum frequency using a lock-in amplifier. This allows us to detect only the contributions to the fluorescence due to the $K(5D,7S)+M$ collisions, where M is an atomic species present in the cell, and we report the rate coefficients for REP with product states $K(4P)+Na(3P_{1/2,3/2})$.

The article is organized in the following way: In Sec. II the experimental setup and density measurement technique are described. In Sec. III a rate-equation model used to extract the reverse energy-pooling rate coefficients from the measured fluorescence intensity ratios and the ground-state atom densities is presented. In Sec. IV we show our experimental results along with a discussion of various sources of error. Finally our conclusions are presented in Sec. V.

II. THE EXPERIMENT

A. Apparatus

Figure 1 shows a schematic overview of the setup used to study the REP processes. The basic features of the experi-

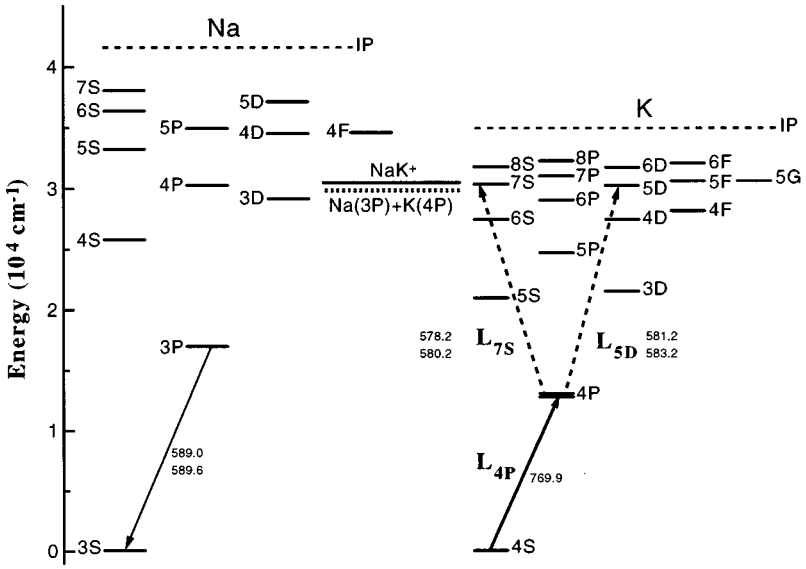

FIG. 2. Energy levels of Na and K. The ionization potential of the two atoms is shown with the dashed line labeled IP. The short dashed lines indicate the energy of the exit channel in reverse energy pooling. The ground well of NaK^+ is also shown according to the data of [19]. Relevant transition are shown with wavelengths in nm.

ment can be described as follows. A capillary glass cell containing a K-Na alloy is heated, creating a mixed alkali-metal vapor in the cell. By propagating two laser beams through the capillary cell, highly excited potassium atoms are produced, some of which will collide with ground-state sodium atoms and transfer a part of their excitation energy to the sodium atoms. The presence of excited sodium atoms gives rise to characteristic fluorescence light, which is collected with a lens, analyzed by a monochromator, and detected with a photomultiplier. The photomultiplier signal is amplified and filtered to extract the part stemming from the collisions between Na and the laser excited K atoms and finally stored on a PC.

The collisions are taking place in a capillary Pyrex cell of length 100 mm, outer diameter 8 mm, and inner diameter 1.8 mm. The tube is closed at both ends with 3-mm-thick Pyrex windows and the center is connected to a bulb filled with a K-Na alloy and sealed under vacuum with a background pressure on the order of 10^{-6} Torr. The alloy in the cell consists of approximately 5% potassium and 95% sodium, and should according to Raoult's law provide approximately equal atom densities and a pressure of 5×10^{-4} Torr at $T \approx 470$ K. A system of narrow slits (0.8×1.5 mm^2) placed on both sides of the tube just after the entrance window defines the volume from which the fluorescence is collected. Thus the collected fluorescence will stem from atoms that have experienced the full laser power.

The cell is placed on top of an electric heater inside a thermally isolated oven. The temperature of the heater is controlled and monitored by a programmable electronic temperature controller using a K-type thermocouple. Another thermocouple, the position of which can be changed during operation, is used to measure the temperature of different parts of the cell. The temperature used for evaluation of the results is measured on the surface of the cell just above the slits (near the entrance window), and this gives an uncertainty in the determination of the absolute gas temperature of 2 K, estimated from the deviation between independent measurements.

The cell was used for a total of about 100 h over a period of several weeks without any visible deterioration of the cell. All rate coefficients were determined from at least five independent measurements and the results could be reproduced within about 25% (cf. Sec. IV). This indicates that the conditions in the cell did not change significantly during its time of usage.

By choosing a small cell diameter it is possible to assure a good overlap of the two beams and a uniform filling of the cell body [15] making the collision area extend over most of the radial part of the cell. In this way the number of atoms not taking part in the collisions is minimized, as is the radiation trapping.

In Fig. 2 the level schemes of the atoms involved are shown. The excitation of the desired potassium levels is accomplished by two broadband dye lasers (bandwidth about 30 GHz) pumped by two cw Ar^+ lasers. The first dye laser (L_{4P}), with Pyridine 2, is operating around the K($4S_{1/2}\rightarrow4P_{1/2}$) transition at 769.9 nm and the second (L_{5D} or L_{7S}), with Rhodamine 110, on the K($4P_{3/2}\rightarrow5D_{5/2}$) transition at 583.2 nm or the K($4P_{1/2}\rightarrow7S_{1/2}$) transition at 578.2 nm. We use these combinations because they give the best signal-to-noise ratio in our experiment. The dye laser frequencies are either manually or computer controlled. Typical laser powers are 300–400 mW.

Before entering the cell each of the laser beams is passed through a set of two lenses so that the beam diameter at the cell entrance is slightly smaller than the cell diameter. The purpose of this is to fill the whole cell volume with light, and at the same time minimize the amount of scattered light from the cell walls. The beams are crossing just after the entrance window of the cell, and due to the small crossing angle, are almost perfectly overlapping through the whole cell volume. The two beams are modulated by a chopper wheel at two

different angular frequencies ω_1 and ω_2 (both prime numbers).

The output power and beam size used give a low laser power density ($5-10\ \mathrm{W/cm^2}$), thus two-photon processes and saturation effects can be safely ignored. We have further verified that we are in the linear regime by measuring the dependence of fluorescence on laser power using neutral-density filters to decrease the laser power.

To resolve the fluorescence coming from the cell spectrally, we use a 0.67-m scanning monochromator (McPherson with 1200-lines/mm grating) with 300-μm slit width. The fluorescence is detected with a Hamamatsu R943-02 photomultiplier, Peltier cooled and operated in photon-counting mode, and the overall spectral response of the system (in the range 400–850 nm) has been determined by passing the white light of a calibrated tungsten lamp through the cell. The signal from the photomultiplier is amplified and discriminated, and then passed to a lock-in amplifier (model SR830 DSP from Stanford Research Systems). By setting the reference frequency of the lock-in to $\omega_r=\omega_1+\omega_2$, the processes induced by the individual lasers are filtered out and only collision processes of the type $\mathrm{K}(5D_J \text{ or } 7S)+M$, where M is any species present in the cell, are recorded.

B. Atom density measurements

The ground-state densities are measured by absorption spectroscopy using a K-Na hollow-cathode (HC) lamp. To measure the density, the light from the lamp is passed through the cell perpendicular to the length axis, using the same slits as for the fluorescence spectra (see Fig. 1), thus measuring the density in the collision volume. The absorption of resonance lines $\mathrm{Na}(3P_J\rightarrow 3S_{1/2})$ and $\mathrm{K}(4P_{1/2}\rightarrow 4S_{1/2})$ from the HC lamp are recorded. The transmitted intensity depends on the ground-state density N according to Beer-Lambert's law, $I=I_0e^{-k_0L}$, where I_0 is the intensity at zero absorption, L is the cell diameter, and k_0 the absorption coefficient at line center. The quantity k_0 can be calculated at a temperature T for a Doppler broadened transition of wavelength λ_0 and radiative decay rate Γ as

$$k_0=N\frac{\lambda_0^2}{8\pi}\frac{g_{\mathrm{up}}}{g_{\mathrm{low}}}\lambda_0\sqrt{\frac{M}{2\pi RT}}\,\Gamma, \tag{8}$$

where g_{up} and g_{low} are the degeneracies of the upper and lower state, respectively, M the atomic mass, and R the gas constant. Thus the ground-state atom density at a given temperature is

$$N(T)=\frac{1}{L}\ln\left(\frac{I_0}{I(T)}\right)\frac{8\pi}{\lambda_0^3}\frac{g_{\mathrm{low}}}{g_{\mathrm{up}}}\sqrt{\frac{2\pi RT}{M}}\frac{1}{\Gamma}. \tag{9}$$

The ground-state density can therefore be determined by measuring the ratio of the intensity of a resonance line after passing through the cell and the intensity at zero absorption. In order to avoid complications of the intensity measurements due to the finite linewidth of the HC lamp, the intensities are evaluated at the center of the absorption lines. We have used the natural radiative decay rates $\Gamma_{3P_{3/2}\rightarrow 3S_{1/2}}=6.10\times10^7\ \mathrm{s}^{-1}$ [16] and $\Gamma_{4P_{1/2}\rightarrow 4S_{1/2}}=3.82\times10^7\ \mathrm{s}^{-1}$ [17] for Na and K, respectively.

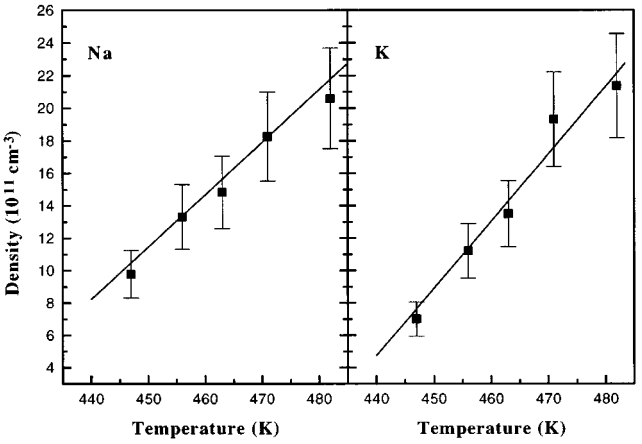

FIG. 3. Measured ground-state densities for Na (left) and K (right). The fit is linear and in good agreement with data from [18].

Before the cell is heated two transmission spectra of the HC lamp are recorded: one around the $\mathrm{Na}(3P_J)$ lines and one around the $\mathrm{K}(4P_{1/2})$ line. The cell is then gradually heated, in order to assure uniform filling of the cell body, and avoid condensation of vapor on the colder parts of the cell. When the temperature is stabilized the two transmission spectra are recorded again.

Figure 3 shows the measured densities of sodium and potassium as a function of temperature using Eq. (9), and we note that the potassium-sodium alloy used gives comparable densities of the two metals in the desired temperature interval. The error in the measurement is mainly due to the uncertainty on the temperature and the instability of the lamp, and it is evaluated as 15%. We note that our measurements are in good agreement with the values calculated according to Raoult's law with 5%-95% K-Na mixture, using vapor pressure curves from Ref. [18].

We also note from Ref. [18] that the densities of molecular dimers at our temperatures are almost three orders of magnitude smaller than those of the single atoms. Thus even if the dimers have broad absorption bands in the visible, we neglect in the following excitation by the dye lasers of $\mathrm{Na_2}$ and NaK, which in principle could produce $\mathrm{Na}(3P_J)$. Our double modulation technique with detection at the sum frequency also filters out signals stemming from dimers, since these signals will only be modulated at the frequency ω_2. In addition, the broadband dye lasers are resonant with the atomic transitions, which have much stronger oscillator strengths than the molecular transitions.

III. RATE EQUATIONS

A. General case

Both of the investigated REP processes described by Eqs. (4) and (5) produce sodium atoms in the $3P_J$ states, and we will use rate equations to derive expressions for the populations of $\mathrm{Na}(3P_J)$ states, which in turn will be used to yield expressions for the REP rate coefficients. The rate equations for our specific case can be written by analyzing Fig. 2 showing the partial energy-level diagram for atomic sodium and potassium together with the sum of the energies of the $\mathrm{Na}(3P_J)$ and the $\mathrm{K}(4P_J)$ levels which constitute the exit channel of the REP reaction. The levels closest to this

TABLE I. Relevant collision processes upon excitation of K($5D$) and K($7S$). The energy defects, given in cm^{-1}, are calculated from [17] using the combination of J levels giving the minimum and maximum ΔE. The AI energy defects are calculated from Refs. [10,19] and ion-pair formation from Refs. [17,20].

Process		Entrance channel→exit channel	Rate	ΔE
Reverse energy	(a)	$K(5D)+Na(3S)\rightarrow K(4P)+Na(3P)$	k_a	170–244
pooling (REP)	(b)	$K(7S)+Na(3S)\rightarrow K(4P)+Na(3P)$	k_b	258–332
Energy transfer	(c)	$K(5D)+Na(3S)\rightarrow K(4S)+Na(4P)$	k_c	(−80)–(−87)
to sodium (ET)	(d)	$K(7S)+Na(3S)\rightarrow K(4S)+Na(4P)$	k_d	2–7
	(e)	$K(5D)+Na(3S)\rightarrow K(4S)+Na(3D)$	k_e	1014
	(f)	$K(7S)+Na(3S)\rightarrow K(4S)+Na(3D)$	k_f	1102
Associative	(g)	$K(5D)+Na(3S)\rightarrow NaK^+ + e^-$	k_g	−230
ionization (AI)	(h)	$K(7S)+Na(3S)\rightarrow NaK^+ + e^-$	k_h	−138
Ion pair	(j)	$K(5D)+Na(3S)\rightarrow K^+ + Na^-$	k_j	−44
formation	(l)	$K(7S)+Na(3S)\rightarrow K^+ + Na^-$	k_l	44

sum are Na($4P$,$3D$) and K($7S$,$5D$,$5F$,$5G$) of which K($7S$ or $5D$) are excited by the lasers in the experiment.

In addition to the REP process the population of Na($3P$) could be due to other processes, e.g., Na($4P$) or Na($3D$) levels produced in a primary collision with K($5D$,$7S$) would decay radiatively through cascade or by secondary collisions to the Na($3P$) levels.

Table I shows the possible collision processes with K($5D$,$7S$) in the entrance channel that are most likely to contribute to the population of Na($3P$), together with the range of energy defects ΔE. Only processes where ΔE is less than a few kT ($kT\sim 330$ cm^{-1} at our temperatures) are included in the table. Energy transfers to potassium atoms are not included in the table since they only contribute to Na($3P$) population via secondary collisions, which can be neglected as shown below. The REP processes (a) and (b) are exothermic by $\sim kT$ while the processes (c) and (d) transferring energy to Na($4P$) are slightly endothermic upon $5D$ excitation but almost resonant upon $7S$ excitation, thus indicating the possibility of a large cross section. The processes (e) and (f) populate the Na($3D$) levels, which can in turn radiate to the Na($3P_J$) levels. These processes are exothermic by almost $3kT$, suggesting a smaller cross section compared with more resonant reactions.

Another contribution to the Na($3P$) signal may be due to recombination of produced ions (NaK^+,$Na_2{}^+$,Na^+) followed by cascade. The ions can be produced through various processes, but since production of $Na_2{}^+$ or Na^+ requires a collision between two excited atoms, the only probable ones are the associative-ionization (AI) processes (g) and (h). AI is seen to be endothermic, but by less than $1kT$ [19]. To our knowledge there are no measurements of ion production in a heteronuclear alkali system with this high excitation. However, we still expect AI to be small compared with the exothermic REP process since production of NaK^+ has to take place at a small internuclear distance. This is corroborated by the observation [21] that AI cross sections in alkalis with initial P-state excitation are of the order 10^{-17} cm^2, and even the largest reported AI process in alkalis [$Cs(7D)+Cs\rightarrow Cs_2{}^+ + e^-$ [22]] would amount to less than 20% of the REP cross sections in our K-Na experiment, and we therefore do not expect AI to distort our results. The other ionization processes that could be considered are ion-pair formation, (j) and (l), where the valence electron of the potassium atom is transferred to the sodium atom. The energy defect is much smaller than kT but neutralization of Na^- will not produce excited Na atoms.

Due to the applied intermodulation technique only radiation stemming from levels prepared directly by the two-step laser excitation or from primary collisional processes involving these levels [K($5D$,$7S$)] are recorded. To discuss the importance of the secondary collisions we note that the atoms in the cell have a thermal mean velocity given by the Maxwell distribution $\langle v\rangle=\sqrt{8kT/\pi M}$ where M is the atomic mass. The mean transit time from wall to wall, in a cylindrical cell of radius $R=0.9$ mm, is hence $\tau_t\sim 2.7$ μs for sodium and $\tau_t\sim 3.0$ μs for potassium at $T=500$ K. The mean time τ_c between atomic collisions can be calculated as $\tau_c=(\sqrt{2}\sigma_c N\langle v\rangle)^{-1}$, where N is the total atomic density, and σ_c is the geometric cross section. Taking the overall atomic density to be 10^{13} cm^{-3}, and 3×10^{-14} cm^2 as a reasonable upper limit for σ_c, this gives a mean free time of $\tau_c\sim 50$ μs. From this it is clear that interatomic collisions are only a small perturbation compared to the wall collisions and that the major contribution to nonradiative decay is collisions with walls. The mean free time is 2–3 orders of magnitude bigger than the typical radiative lifetimes [23]. Thus it is unlikely for an atom that has been excited by a collision process to collide again before it is deexcited by radiative decay, and we therefore also neglect secondary collisions. Thus processes such as energy transfer in sodium

$$Na(4P)+M\rightarrow Na(3D)+M \tag{10}$$

and fine-structure mixing

$$Na(3P_J)+M\rightarrow Na(3P_{J'})+M \tag{11}$$

will not be considered important in our experiment although their cross sections are rather large [$\approx(100-200)\times 10^{-16}$ cm^2] [24,25].

Following the discussion above, the steady-state rate equations for the Na($3P_J$) levels are

$$[\mathrm{Na}]_{3P_J}=0=k_a[\mathrm{K}]_{5D}[\mathrm{Na}]_{3S}+\sum_{nl_J}\Gamma_{nl_J-3P_J}[\mathrm{Na}]_{nl_J}-\Gamma_{3P_J-3S_{1/2}}[\mathrm{Na}]_{3P_J}, \quad (12)$$

and

$$[\mathrm{Na}]_{3P_J}=0=k_b[\mathrm{K}]_{7S}[\mathrm{Na}]_{3S}+\sum_{nl_J}\Gamma_{nl_J-3P_J}[\mathrm{Na}]_{nl_J}-\Gamma_{3P_J-3S_{1/2}}[\mathrm{Na}]_{3P_J}, \quad (13)$$

for the case of $5D$ and $7S$ excitation, respectively. $[N]_{nl_J}$ is the density of atoms in the state nl_J, and $\Gamma_{nl_J-n'l'_{J'}}$ is the effective radiation rate from level nl_J to level $n'l'_{J'}$. The effective radiation rate can be calculated as $\Gamma^{\mathrm{eff}}=\overline{g}\Gamma^{\mathrm{nat}}$, where $\overline{g}$ is the average probability of a photon escaping from anywhere in the cell into any direction, and Γ^{nat} is the natural radiative rate. In order to simplify the notation the decay rates are not labeled according to the atomic species they belong to, since this should be clear from the context. The first term on the right-hand side of Eqs. (12) and (13) gives the population rate of the REP processes, the second term gives the population rate due to radiation from higher-lying sodium levels, and the last term the depopulation rate due to radiative decay.

The measured fluorescence intensities are given by

$$I_{nl_J-n'l'_{J'}}=\epsilon(\nu)h\nu_{nl_J-n'l'_{J'}}[N]_{nl_J}\Gamma_{nl_J-n'l'_{J'}}V\frac{\Omega}{4\pi}, \quad (14)$$

where V is the volume from which fluorescence is observed, Ω the solid angle of observation, $\nu_{nl_J-n'l'_{J'}}$ the transition frequency, $\Gamma_{nl_J-n'l'_{J'}}$ the effective radiative rates (in the direction of observation), and $\epsilon(\nu)$ the spectral response of the system at the given wavelength. Assuming that different transitions are observed from the same volume, which is assured by our experimental arrangement, we obtain rate equations not depending on the volume or angle of observation.

To evaluate the term on the right-hand sides of Eqs. (12) and (13) it is necessary to measure the fluorescence intensities stemming from the laser-populated high level [K($5D$) or K($7S$)] to a lower state [K($4P$)] and from the REP populated level [Na($3P$)] to the ground level [Na($3S$)]. It is also necessary to determine the density of ground-state sodium atoms. The effective radiation rates for the K($5D,7S\rightarrow 4P$) transitions at the present experimental conditions can be shown to be equal to the corresponding Einstein coefficients to a very good approximation [14].

B. K($5D$) excitation

The highest absorption coefficient for exciting the $5D$ level is that of the K($4P_{3/2}\rightarrow 5D_{5/2}$) transition but since the fine-structure splitting is only 0.5 cm^{-1} our broadband laser also excites the K($4P_{3/2}\rightarrow 5D_{3/2}$) transition. We will assume that the relative population distribution between K($5D_{3/2}$) and K($5D_{5/2}$) levels is fully thermalized:

$$\frac{[\mathrm{K}]_{5D_{5/2}}}{[\mathrm{K}]_{5D_{3/2}}}=\frac{(2\times 5/2+1)}{(2\times 3/2+1)}e^{-[E(5D_{5/2})-E(5D_{3/2})]/kT}\approx 3/2, \quad (15)$$

where $E(5D_{5/2})$ and $E(5D_{3/2})$ are the energies of the K($5D_{3/2}$) and K($5D_{5/2}$) levels, respectively. By introducing intensity ratios and using the relation $[\mathrm{K}]_{5D}=[\mathrm{K}]_{5D_{5/2}}+[\mathrm{K}]_{5D_{3/2}}=(5/2)[\mathrm{K}]_{5D_{3/2}}$, the steady-state rate equation (12) can be rewritten to express the rate coefficients for the REP processes as

$$k_a+\frac{1}{[\mathrm{K}]_{5D}[\mathrm{Na}]_{3S_{1/2}}}\sum_{nl_J}\Gamma_{nl_J}[\mathrm{Na}]_{nl_J}=\frac{2}{5}\left(\frac{I_{3P_J-3S_{1/2}}}{I_{5D_{3/2}-4P_{1/2}}}\right)_c\frac{\nu_{5D_{3/2}-4P_{1/2}}\Gamma_{5D_{3/2}-4P_{1/2}}}{\nu_{3P_J-3S_{1/2}}}\frac{1}{[\mathrm{Na}]_{3S_{1/2}}}. \quad (16)$$

The subscript c indicates that the intensity ratios have been corrected for the spectral response ϵ of the detection system.

The second term on the left-hand side of Eq. (16) is connected with radiative population of the Na($3P_J$) level through radiation from higher levels in sodium. When population is transferred to the Na($4P_J$) level [by processes (c)] or to Na($3D_J$) [by process (f)] all the lower-lying levels will in turn be populated, either by direct radiation or by cascading. To determine this contribution to the Na($3P_J$) level population the steady-state rate equations for these higher-lying levels must be examined. According to the rate of interatomic collisions, the dominant deactivation process for collisionally populated levels will be radiation. For Na($4P_J$) this gives the rate equation

$$[\mathrm{Na}]_{4P_J}=0=k_c[\mathrm{K}]_{5D}[\mathrm{Na}]_{3S_{1/2}}-\sum_{nl_{J'}}\Gamma_{4P_J-nl_{J'}}[\mathrm{Na}]_{4P_J}. \quad (17)$$

From Eq. (17), summing over all the transition probabilities we obtain, for the $4P_{3/2}$ state of sodium, the following steady-state solution:

$$[\mathrm{Na}]_{4P_{3/2}}\approx 1.03\times 10^{-7}k'_c[\mathrm{K}]_{5D}[\mathrm{Na}]_{3S_{1/2}}, \quad (18)$$

where k'_c denotes the rate constant for only the part of process (c) contributing to the population of the 3/2 component. Assuming a statistical ratio we have $k'_c=2/3k_c$. Under the assumption that the radiation from the $4P_{3/2}$ level is the dominant process in populating the $4S_{1/2}$, $3D_{3/2}$, and $3D_{5/2}$ states in sodium we obtain the following relations for the densities of these states:

$$[\mathrm{Na}]_{4S_{1/2}}=\frac{\frac{1}{2}\Gamma_{4P_{1/2}-4S_{1/2}}+\Gamma_{4P_{3/2}-4S_{1/2}}}{\Gamma_{4S_{1/2}-3P_{1/2}}+\Gamma_{4S_{1/2}-3P_{3/2}}}[\mathrm{Na}]_{4P_{3/2}}\approx 0.390[\mathrm{Na}]_{4P_{3/2}}, \quad (19)$$

$$[\mathrm{Na}]_{3D_{3/2}}=\frac{\frac{1}{2}\Gamma_{4P_{1/2}-3D_{3/2}}+\Gamma_{4P_{3/2}-3D_{3/2}}}{\Gamma_{3D_{3/2}-3P_{1/2}}+\Gamma_{3D_{3/2}-3P_{3/2}}}[\mathrm{Na}]_{4P_{3/2}}$$
$$\approx 9.38\times 10^{-4}[\mathrm{Na}]_{4P_{3/2}}, \tag{20}$$

$$[\mathrm{Na}]_{3D_{5/2}}=\frac{\Gamma_{4P_{3/2}-3D_{5/2}}}{\Gamma_{3D_{5/2}-3P_{3/2}}}[\mathrm{Na}]_{4P_{3/2}}\approx 1.41\times 10^{-3}[\mathrm{Na}]_{4P_{3/2}}. \tag{21}$$

For the Na($3D_J$) we have the rate equation

$$[\mathrm{Na}]_{3D_J}=0=k_e[\mathrm{K}]_{5D}[\mathrm{Na}]_{3S_{1/2}}-\sum_{nl_{J'}}\Gamma_{3D_J-nl_{J'}}[\mathrm{Na}]_{3D_J}. \tag{22}$$

From Eq. (22) for Na($3D_{5/2}$) we obtain the following rate equation where k_e' denotes the rate constant only for the part of process (e) populating the 5/2 component:

$$[\mathrm{Na}]_{3D_{5/2}}=\Gamma^{-1}_{3D_{5/2}-3P_{3/2}}k_e'[\mathrm{K}]_{5D}[\mathrm{Na}]_{3S_{1/2}}. \tag{23}$$

Assuming again a statistical ratio among the Na($3D_J$) states we have that $k_e'=3/5k_e$. Moreover we note that the $3D_J$ states can radiate only to the Na($3P_J$) so using the relations (17), (19)–(21), and (23). we evaluate the second term on the left-hand side of Eq. (16), and obtain

$$\frac{1}{[\mathrm{K}]_{5D}[\mathrm{Na}]_{3S_{1/2}}}\cdot\sum_{nl_J}\Gamma_{nl_J}[\mathrm{Na}]_{nl_J}=0.685\times\frac{2}{3}k_c+0.6k_e, \tag{24}$$

$$\frac{1}{[\mathrm{K}]_{5D}[\mathrm{Na}]_{3S_{1/2}}}\cdot\sum_{nl_J}\Gamma_{nl_J}[\mathrm{Na}]_{nl_J}=0.341\times\frac{2}{3}k_c+0.4k_e \tag{25}$$

for Na($3P_{3/2}$) and Na($3P_{1/2}$), respectively.

Inserting Eqs. (24) and (25) in the steady-state rate equations (16) we obtain

$$k_a+0.46k_c+0.6k_e$$
$$=67982.0\ \mathrm{s}^{-1}\times\left(\frac{I_{3P_{3/2}-3S_{1/2}}}{I_{5D_{3/2}-4P_{1/2}}}\right)_c\frac{1}{[\mathrm{Na}]_{3S_{1/2}}}, \tag{26}$$

$$k_a+0.23k_c+0.4k_e=68050.9\ \mathrm{s}^{-1}\times\left(\frac{I_{3P_{1/2}-3S_{1/2}}}{I_{5D_{3/2}-4P_{1/2}}}\right)_c\frac{1}{[\mathrm{Na}]_{3S_{1/2}}} \tag{27}$$

for the Na($3P_{3/2}$) and the Na($3P_{1/2}$) levels, respectively. Note that the above expressions for k_a do not (to a good approximation [14]) depend on the effective radiation rate $\Gamma_{3P_J\rightarrow 3S_{1/2}}$, which could be affected by radiation trapping. The numerical factor on the right-hand side is obtained from $\frac{2}{5}(\nu_{5D_{3/2}-4P_{1/2}}\Gamma_{5D_{3/2}-4P_{1/2}})/\nu_{3P_J-3S_{1/2}}$, where $\Gamma_{5D_{3/2}-4P_{1/2}}$ is taken from Ref. [23].

We note that we have an intensity ratio in Eqs. (26) and (27). This is an advantage since we do not have to consider geometrical effects. We recall that since the cell is fully illuminated by the laser the spatial distribution of K($5D$) is expected to be isotropic. However, because the radiative lifetime and the diffusion time for the K($5D$) atoms are of the same magnitude, diffusion of K($5D$) has to be considered. The intensity of the K($5D\rightarrow 4P$) lines decreases because of the losses from collisions with the cell walls. However, the same losses also reduce the production of Na($3P$) by the same fraction.

C. K($7S$) excitation

In the case of K($7S$) excitation the second laser is tuned to the K($4P_{1/2}\rightarrow 7S_{1/2}$) transition giving a different excitation scheme. Rearranging Eq. (13) in terms of convenient intensity ratios, the steady-state rate equation can be written in a form similar to the case of K($5D$) excitation

$$k_b+\frac{1}{[\mathrm{Na}]_{3S_{1/2}}[\mathrm{K}]_{7S_{1/2}}}\sum_{nl_J}\Gamma_{nl_J}[\mathrm{Na}]_{nl_J}$$
$$=\left(\frac{I_{3P_J-3S_{1/2}}}{I_{7S_{3/2}-4P_{1/2}}}\right)_c\cdot\frac{\nu_{7S_{1/2}-4P_{3/2}}\cdot\Gamma_{7S_{1/2}-4P_{3/2}}}{\nu_{3P_J-3S_{1/2}}}\cdot\frac{1}{[Na]_{3S_{1/2}}}, \tag{28}$$

The second term on the left-hand side of Eq. (28) can be evaluated like in the K($5D$) excitation case, with $[\mathrm{K}]_{7S_J}$ replacing $[\mathrm{K}]_{5D_J}$, k_d replacing k_c, and k_f replacing k_e. The steady-state rate equations for the Na($3P_{3/2}$) and the Na($3P_{1/2}$) levels hence yield

$$k_b+0.46k_d+0.6k_f$$
$$=2.061\times 10^6\ \mathrm{s}^{-1}\times\left(\frac{I_{3P_{3/2}-3S_{1/2}}}{I_{7S_{1/2}-4P_{1/2}}}\right)_c\frac{1}{[\mathrm{Na}]_{3S_{1/2}}} \tag{29}$$

and

$$k_b+0.23k_d+0.4k_f$$
$$=2.063\times 10^6\ \mathrm{s}^{-1}\times\left(\frac{I_{3P_{1/2}-3S_{1/2}}}{I_{7S_{1/2}-4P_{1/2}}}\right)_c\frac{1}{[\mathrm{Na}]_{3S_{1/2}}}, \tag{30}$$

respectively.

IV. FLUORESCENCE MEASUREMENTS AND RESULTS

The intensity ratios necessary to evaluate the rate constants have been obtained by scanning the monochromator in the range (588.8–590.5 nm) around the Na($3P_J\rightarrow 3S_{1/2}$) transitions and in the range (580.0–582.0 nm) around the K($7S_{1/2}\rightarrow 4P_{3/2}$) and K($5D_{3/2}\rightarrow 4P_{1/2}$) transitions. Appropriate neutral density filters have been used since the intensities differ by about three orders of magnitude.

Figure 4 shows spectra recorded at 481 K (a) and recorded at 466 K (b) in the case of $5D$-state laser excitation. The left spectrum shows two potassium lines: one line originating from the K($5D_{3/2}$) level, which is populated directly by the lasers, and the another line from the K($7S_{1/2}$) level, which is populated by the energy-transfer process

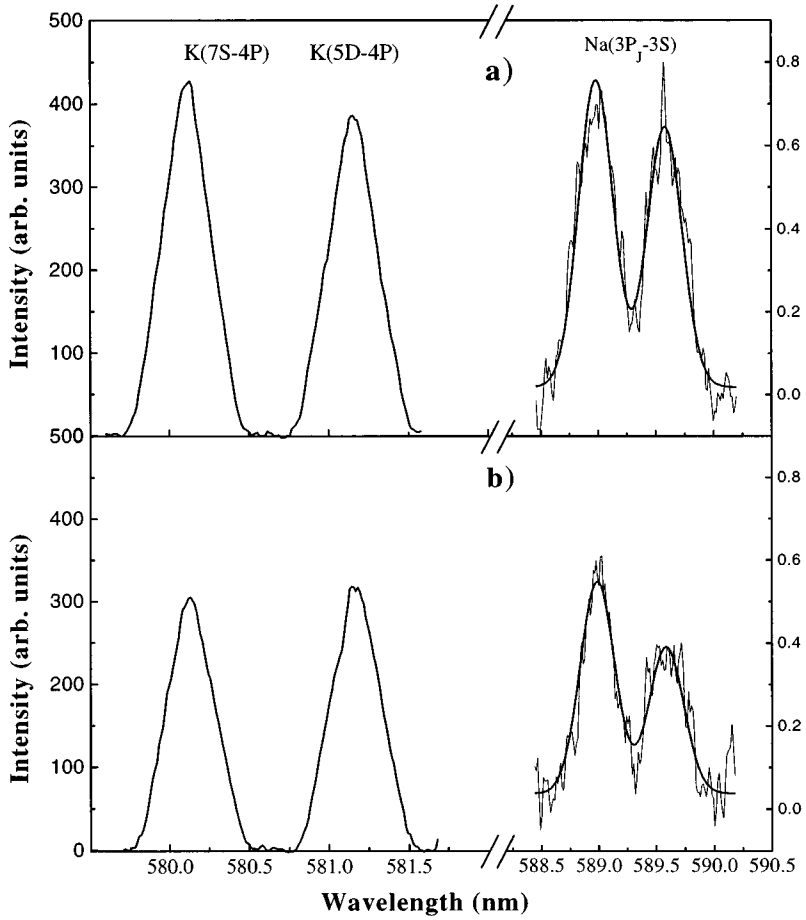

FIG. 4. Fluorescence spectra recorded at 481 K (a) and at 466 K (b) in the case of $5D$ excitation. The left spectra show the potassium lines and the right ones are the sodium D lines. The sodium lines are fitted with two Gaussians.

$$\mathrm{K}(5D)+\mathrm{Na}(3S),\ \ \mathrm{K}(4S)\rightarrow\mathrm{K}(7S)+\mathrm{Na}(3S),\ \ \mathrm{K}(4S). \tag{31}$$

The right spectrum shows the emission from Na($3P_J$) levels, which are the product of REP process (a). One can see that the ratio of $5D$-$4P$ to $7S$-$4P$ fluorescence changes only slightly with the changing temperature and is approximately one. However, a trend showing an increasing population of the $7S$ state can be seen as the atom density increases. More pronounced is the change of intensity ratio of the Na $D2$ and $D1$ lines. This could be either due to trapping, which is more pronounced on the $D2$ line or due to the change in relative population of $\mathrm{Na}_{3P_{3/2}}$ and $\mathrm{Na}_{3P_{1/2}}$ levels.

Figure 5 shows spectra recorded at 481 K (a) and recorded at 458 K (b) in the case of $7S$-state laser excitation. The left spectrum shows two potassium lines, one stemming from the K($7S_{1/2}$) level, which is populated directly by the lasers, and the other from the K($5D_{3/2}$) level, which is populated by the energy-transfer process

$$\mathrm{K}(7S)+\mathrm{Na}(3S),\ \ \mathrm{K}(4S)\rightarrow\mathrm{K}(5D)+\mathrm{Na}(3S),\ \ \mathrm{K}(4S). \tag{32}$$

The right spectrum shows emission from the Na($3P_J$) levels which are the product of REP process (b). In this case of excitation the intensity ratio between $7S$ and $5D$ is about 1000 and also does not change significantly with temperature. Also in the case of $7S$ excitation we observe a change in the ratio of Na($3P_J$) emission.

In order to evaluate the intensity ratios needed in Eqs. (26), (27), (29), and (30) the measured line shapes were fitted by Gaussian curves of fixed half-width and separation. This allowed us to subtract a linear background around the Na D lines, which was found to be up to 10% of the maximum measured intensities at lowest temperatures. This background may be due to laser broadband emission (amplified spontaneous emission) and to scattering from the capillary cell. The oscillations in the emission spectra are due to the limited dynamic reserve of the lock-in amplifier.

Figure 6 shows the measured values of rate coefficients calculated from the rate equations (26), (27), (29), and (30). The rate constants contain contributions from both exit channels K($4P_J$), which cannot be separated in the experiment, because they are involved in the laser-excitation path. The rate constants for the two Na($3P_J$) exit channels are almost equal for the highest temperatures in both cases of excitation, while for decreasing temperatures the ratio between the rate constants for the Na($3P_{3/2}$) and the Na($3P_{1/2}$) exit channels increases slightly. In both cases of laser excitation a temperature dependence of the rate coefficients is observed, which, however, is more pronounced for $5D$ excitation than for $7S$ excitation.

In the case of 5D excitation we obtain averaged rate coefficients at the mean temperature $T=465\,\mathrm{K}$ as k_a

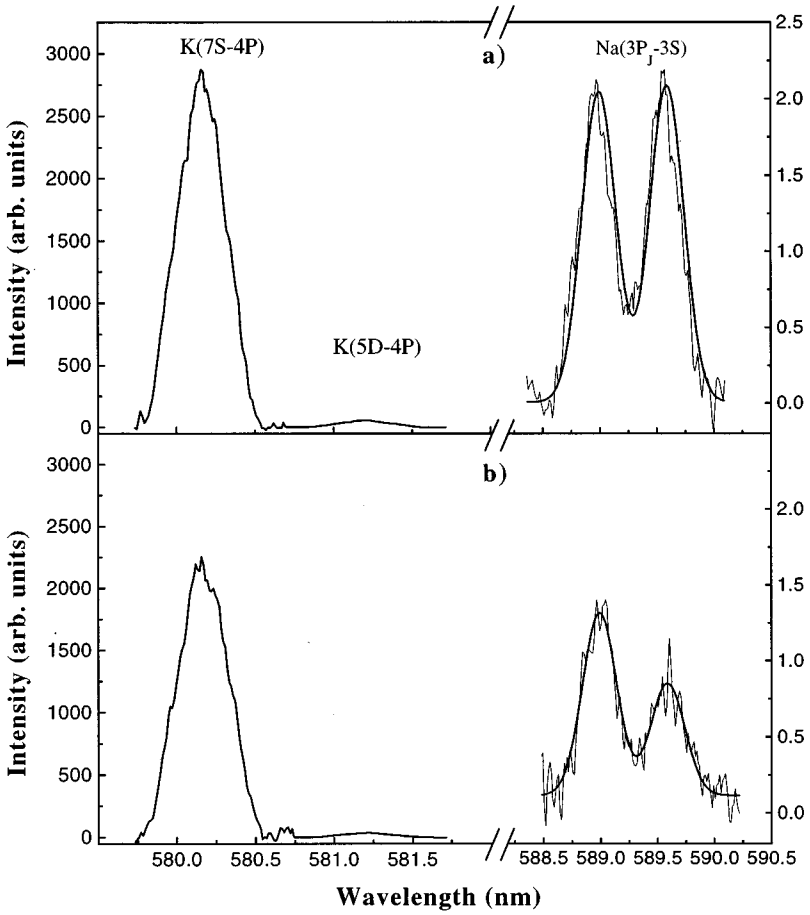

FIG. 5. Fluorescence spectra recorded at 481 K (a) and at 466 K (b) in the case of $7S$ excitation. The left spectra show the potassium lines and the right ones are the sodium D lines. The sodium lines are fitted with two Gaussians.

$=1.1\times10^{-9}$ and 0.8×10^{-9} cm^3 s^{-1} for the K($4P_J$) + Na($3P_{3/2}$) and K($4P_J$) + Na($3P_{1/2}$) exit channels, respectively. The cross sections, related to the rate coefficients by the interatomic mean velocity, are then $\sigma_a=125\times10^{-16}$ and 95×10^{-16} cm^2, respectively. For $7S$ excitation we obtain $k_b=2.2\times10^{-9}$ and 1.4×10^{-9} cm^3 s^{-1} for the K($4P_J$) + Na($3P_{3/2}$) and K($4P_J$) + Na($3P_{1/2}$) channels, respectively. The related cross sections are $\sigma_b=270\times10^{-16}$ and 175×10^{-16} cm^2, respectively.

The uncertainty on the values in Fig. 6 has been given as the standard deviation of values determined from several independent measurements. This uncertainty can be attributed to the uncertainties of the experimentally determined quantities appearing in the simplified rate equations: The uncertainty on the fluorescence ratios were determined by performing several independent measurements to be about 25%, probably mostly due to instability of the lasers. From a comparison of available literature data on measurements of the natural decay rates used in the evaluation of the rate constants, these where found to have an uncertainty of about 20%. Adding in quadrature this gives an overall (statistical) uncertainty of 45%, which is comparable to the uncertainties usually found in these kinds of measurements.

According to the rate equation model the radiative decay from levels populated by the energy-transfer processes [(c), (d)] and [(e), (f)], contribute to the Na($3P_J$) population with 20–40% of $k_{c,d}$ and 40–60% of $k_{e,f}$ depending on the excitation scheme and the considered J level. From Landau-Zener calculations (Ref. [13]) k_c is found to be more than one order of magnitude smaller than k_a, and if we assume $k_d \approx k_c$ the contribution from these processes is then of the same magnitude as the secondary REP processes. We have tried to determine $k_{c,d}$ by looking for fluorescence from the Na($4P_J \rightarrow 3S_{1/2}$) transition at 330.4 nm, which is at the limit of our detection sensitivity, but we were not able to distin-

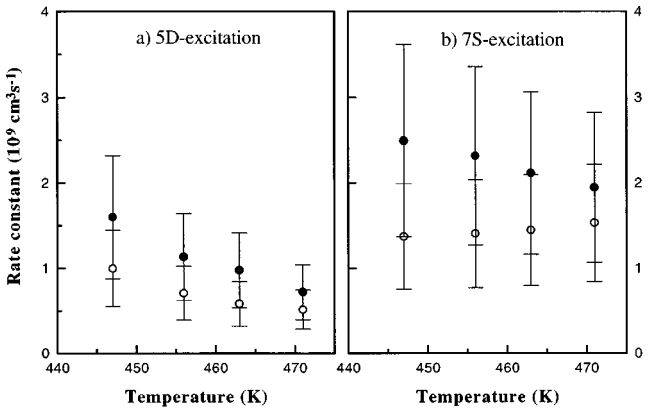

FIG. 6. Measured rate constants for the REP processes for the $5D$ (left) and $7S$ (right) excitation. The open circles are rates for Na($3P_{1/2}$) and the closed circles are for the Na($3P_{3/2}$) population.

TABLE II. Cross sections for energy-pooling and reverse energy-pooling collisions in KNa.

Process	$\sigma(10^{-16}\ \mathrm{cm}^2)$	T (K)	Reference
$K(4P)+Na(3P)\rightarrow K(4S)+Na(3D)$	28 ± 14	513	[3]
$K(4P)+Na(3P)\rightarrow K(5D)+Na(3S)$	38 ± 19	513	[3]
$K(4P)+Na(3P)\rightarrow K(7S)+Na(3S)$	18 ± 9	513	[3]
$K(5D)+Na(3S)\rightarrow K(4P_J)+Na(3P_{1/2})$	95 ± 45	465	This work
$K(5D)+Na(3S)\rightarrow K(4P_J)+Na(3P_{3/2})$	125 ± 55	465	This work
$K(5D)+Na(3S)\rightarrow K(4P)+Na(3P)$	220 ± 100	465	This work
$K(7S)+Na(3S)\rightarrow K(4P)+Na(3P_{1/2})$	175 ± 80	465	This work
$K(7S)+Na(3S)\rightarrow K(4P)+Na(3P_{3/2})$	270 ± 120	465	This work
$K(7S)+Na(3S)\rightarrow K(4P)+Na(3P)$	445 ± 200	465	This work
$K(5D)+Na(3S)\rightarrow K(4P)+Na(3P)$	400	465	[13]

guish signal from noise. The cross section for process (e) has been evaluated theoretically and it is less than 20×10^{-16} cm^2 in our range of temperatures [26,27]. Assuming that $k_f\approx k_e$ also the contribution of process (f) is negligible compared with the size of the REP rate constant. We have also looked for transitions from the $Na(3D_J)$ level that have an energy defect of almost $3kT$. The fact that we did not see any fluorescence from these levels does not prove that there is no radiation contribution to the $Na(3P_J)$ population, but it indeed indicates that it is so small that it can be neglected.

Based on the intensity ratios of $5D$ to $7S$ emission we can also estimate that the contribution of secondary collisions, e.g., in the case of $5D$ excitation, from $K(7S)+Na(3S)$, does not exceed 5%.

V. DISCUSSION

In Table II we show the cross sections for direct and reverse energy-pooling collisions in the K-Na system. Note that the values reported in [3] must be corrected by a factor of 2 because they were measured relative to the homonuclear energy-pooling process $Na(3P)+Na(3P)\rightarrow Na(3S)+Na(5S)$, which must be corrected to avoid double counting of atom pairs [28]. In the study of the forward process none of the fine-structure components were resolved, and the measurements were performed at a temperature ~50 K higher than in the present case. To compare the EP cross sections with the present REP results we have to sum contributions for both $K(4P_J)+Na(3P_{3/2})$ and $K(4P_J)+Na(3P_{1/2})$ exit channels. In Fig. 7 we have reproduced the exothermic side of Fig. 3 in Ref. [4] and included later measurements on alkali metals [9]. The rate constants are displayed versus the energy defect and the REP rate constants obtained from the present work have been added. Our data fit well into the general picture noted by Gabbanini *et al.* [4] that the order of magnitude of the rate coefficients depends on the fundamental parameter $\Delta E/k_BT$, and in the form of the exponential decay function in Eq. (3). The new data allow us to improve the fit in Ref. [4], giving the values $A=(5.0\pm0.6)\times10^{-9}$ cm^3 s^{-1} and $B=1.2\pm0.3$ in Eq. (3). From this result we suggest that a simpler functional dependance of k on $\Delta E/k_BT$ can be obtained by fixing $B=1$ in Eq. (3). A fit to the data gives again $A=(5.0\pm0.6)\times10^{-9}$ cm^3 s^{-1}. This new fit is also displayed in Fig. 7.

We recall that our data showed the exit channel $K(4P_J)+Na(3P_{3/2})$ to be favored over the $K(4P_J)+Na(3P_{1/2})$ channel both in the case of REP with $K(7S)$ and with $K(5D)$. The largest difference in the rate between the two exit channels is with initial $K(7S)$ excitation. This could suggest a role played by the angular momentum as observed by Namiotka *et al.* [29] for $K(4P_J)+K(4P_J)$ energy pooling, suggesting an angular momentum propensity rule. In that study it was possible to relate the population of the $K(6S)$ state with the $K(4P_{3/2})+K(4P_{3/2})$ entrance channel and $K(5P)$ with the $K(4P_{1/2})+K(4P_{1/2})$ entrance channel. The difference in rates was approximately a factor 2.7.

In the present experiment for the case of $K(7S)$ excitation the entrance channel is well defined $[K(7S_{1/2})+Na(3S_{1/2})]$ and we observe a difference in rates by a factor of 1.6. For $K(5D)$ excitation the experiment does not select the J sublevel of the $5D$ state and the entrance channel is thus less well defined $[K(5D_{3/2,5/2})+Na(3S_{1/2})]$. In this case a smaller difference in rates (a factor of 1.3) is observed, and it is possible that this smaller propensity is due to the fact that the initial state is prepared in a mixture of $K(5D_{3/2})$ and $K(5D_{5/2})$.

A rough calculation of the REP rate coefficients can be made using the principle of detailed energy balance. Taking

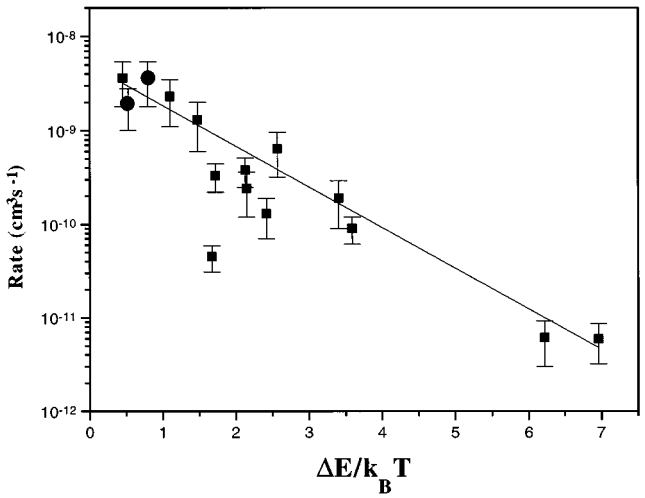

FIG. 7. Plot of the rate constant experimental values vs $\Delta E/k_BT$ for the exothermic cases. The points measured in this work are indicated with a circle and the line represents an exponential decay fit.

the average values for the energies of entrance $K(4P)+Na(3P)$ ($E_{EP}=29978.8\ cm^{-1}$) and exit channels $K(5D)+Na(3S)$ ($E_{REP}=30185.49\ cm^{-1}$) and $K(7S)+Na(3S)$ ($E_{REP}=30274.26\ cm^{-1}$). For $5D$ excitation we thus use the relation

$$\frac{\sigma_{EP}}{\sigma_{REP}}=\frac{5}{9}e^{[-297.4/T(K)]} \tag{33}$$

and the value $\sigma_{EP}=(38\pm19)\times10^{-16}\ cm^2$ [3] to obtain $\sigma_{REP}^{db}=(140\pm70)\times10^{-16}\ cm^2$. Similarly, for $7S$ excitation, according to

$$\frac{\sigma_{EP}}{\sigma_{REP}}=\frac{1}{9}e^{[-425.1/T(K)]} \tag{34}$$

and using the value $\sigma_{EP}=(18\pm9)\times10^{-16}\ cm^2$ [3] we obtain $\sigma_{REP}^{db}=(400\pm200)\times10^{-16}\ cm^2$. These results give a reasonable agreement with our measured values within the large error bars in both experiments and may be used as an indicator that only a few exit channels are open. We note that looking, in the framework of the detailed balance principle, at forward and reverse EP cross sections, a much larger difference is expected for $S+S\rightarrow P+P$ collisions than for $D+S\rightarrow P+P$ collisions simply due to the ratio of relevant statistical weights. The cross sections for the REP (exothermic) processes appear to be an order of magnitude bigger than for the EP (endothermic) processes, which is in accordance with the empirical behavior of EP cross sections discussed in Ref. [4].

In a preliminary report [13] the Landau-Zener model was used to calculate the cross section for the $K(5D)+Na(3S)\rightarrow K(4P)+Na(3P)$ process. The theoretical treatments did not include the fine-structure interaction in the calculation of the potential-energy curves, and for this reason we can only compare the theoretical results with the total experimental cross section for the reverse energy pooling obtained as we described above by summing the cross sections for the two exit channels. The result is summarized in Table II and shows that the model reproduces the experimental result within a factor of two, which is a resonable result for a semiclassical calculation. The model also predicts a much larger cross section for the $K(4P)+Na(3P)$ exit channel than for any other [13]. Also this result supports our observation. We note that an advantage of the present experiment is that dealing with such a large cross section, the experiment can be performed at sufficiently low atom density to neglect the fine-structure mixing collisions $Na_{3P_{3/2}\leftrightarrow3P_{1/2}}$ and $K_{4P_{3/2}\leftrightarrow4P_{1/2}}$ as shown in the work by Davidson *et al.* [30].

The observed temperature dependence of the rate coefficients was also discussed in our preliminary report [13]. We recall here that the temperature dependence is relatively pronounced for the $K(4P_J)+Na(3P_{3/2})$ channels in the case of $5D$ excitation and less strong for the $K(4P_J)+Na(3P_{1/2})$ channel, while the dependence is much weaker for the two channels with $7S$ excitation. As discussed in [13] several effects can cause a decrease of the rate coefficients with increasing temperature.

In summary we have observed heteronuclear reverse energy pooling and measured the rate coefficients for the processes $K(5D,7S)+Na(3S)\rightarrow K(4P)+Na(3P_J)$. A good agreement with a semiclassical Landau-Zener model is obtained considering the combined experimental and model uncertainties.

Since our experiment was performed in a sealed cell, we could not easily modify the setup to detect production of ions in the collisions. As discussed in Sec. IV this is one of the uncertainties in the experiment, and we have therefore constructed a new apparatus [31] where collisions between excited atoms can be studied in atomic beams. The planned experiment will allow a measurement of associative ionization and ion-pair formation in homonuclear and heteronuclear collisions and will thus complement the information obtained in the cell experiments.

ACKNOWLEDGMENTS

This work was supported by the Danish Natural Science Research Council, Ib Henriksens Foundation (Copenhagen), and by the EEC-HCM program (Contract No. ERBCHRXCT 930344). S.M. thanks the Danish Natural Science Research Council for financial support during his stay in Copenhagen and J.O.P.P. thanks the Carlsberg Foundation for financial support during the finishing of this manuscript. Finally, we thank Nils Andersen and John Huennekens for useful discussions, and we also thank Nils Andersen for lending us most of the equipment used in the experiment.

[1] M. Allegrini, G. Alzetta, A. Kopystynska, L. Moi, and G. Orriols, Opt. Commun. **19**, 96 (1976).
[2] M. Allegrini, P. Bicchi, S. Gozzini, and P. Savino, Opt. Commun. **36**, 445 (1981).
[3] S. Gozzini, S. A. Abdullah, M. Allegrini, A. Cremoncini, and L. Moi, Opt. Commun. **36**, 97 (1987).
[4] C. Gabbanini, S. Gozzini, G. Squadrito, M. Allegrini, and L. Moi, Phys. Rev. A **39**, 6148 (1989).
[5] J. T. Bahns, M. Koch, and W. C. Stwalley, in *The Physics of Ionized Gases*, edited by L. Tanovic, N. Konjevic, and N. Tanovic (Nova Science Publishers, Commack, NY, 1989).
[6] D. Veza and C. J. Sansonetti, Z. Phys. D **22**, 463 (1992).
[7] G. Pichler (private communication).
[8] T. Yabuzaki, A. C. Tam, M. Hou W. Happer, and S. M. Curry, Opt. Commun. **24**, 305 (1978).
[9] Z. J. Jabbour, R. K. Namiotka, J. Huennekens, M. Allegrini, S. Milosevic, F. de Tomasi, Phys. Rev. A **54**, 1372 (1996).
[10] S. Magnier and Ph. Millie, Phys. Rev. A **54**, 204 (1996).
[11] P. Brumer and M. Shapiro, Sci. Am. (Int. Ed.) **272** (March) 34 (1995).
[12] M. Shapiro and P. Brumer, Phys. Rev. Lett. **77**, 2574 (1996).
[13] S. Guldberg-Kjær, G. De Filippo, S. Milosevic, S. Magnier, J. O. P. Pedersen, M. Allegrini, Phys. Rev. A **55**, R2515 (1997).
[14] S. A. Guldberg-Kjær, M.Sc. thesis, University of Copenhagen, 1996 (unpublished).

[15] M. Allegrini, P. Bicchi, and L. Moi, Phys. Rev. A **28**, 1338 (1983).
[16] A. Gaupp, P. Kuske, and H. J. Andrä, Phys. Rev. A **26**, 3351 (1982).
[17] C. E. Moore, *Atomic Energy Levels, Vol. I* (National Bureau of Standards, Washington, D.C., 1949).
[18] A. N. Nesmeyanov, *Vapor Pressure of the Chemical Elments* (Elsevier, Amsterdam, 1963).
[19] S. Leutwyler, M. Hofmann, H.-P. Harri, and E. Schumacher, Chem. Phys. Lett. **77**, 257 (1981).
[20] T. A. Patterson, H. Hotop, A. Kasdan, D. W. Norcross, and W. C. Lineberger, Phys. Rev. Lett. **32**, 189 (1974).
[21] M. Allegrini, C. Gabbanini, and L. Moi, J. Phys. (Paris), Colloq. **46**, C1-61 (1985).
[22] B. V. Dobrolezh, A. N. Klyucharev, and V. Yu Sepman, Opt. Spektrosk. **38**, 1090 (1975) [Opt. Spectrosc. **38**, 630 (1975)].
[23] B. Warner, Mon. Not. R. Astron. Soc. **139**, 115 (1968).
[24] V. Horvatic, D. Veza, M. Movre, K. Niemax, and C. Vadla, Z. Phys. D **34**, 163 (1995).
[25] J. Huennekens and A. Gallagher, Phys. Rev. A **27**, 1851 (1983).
[26] I. Yu Yurova (private communication).
[27] M. Lundsgaard (private communication).
[28] N. N. Bezuglov, A. N. Klucharev, and V. A. Shereverev, J. Phys. B **20**, 2497 (1987).
[29] R. K. Namiotka, J. Huennekens, and M. Allegrini, Phys. Rev. A **56**, 514 (1997).
[30] S. A. Davidson, J. F. Kelly, and A. Gallagher, Phys. Rev. A **33**, 3756 (1986).
[31] S. Guldberg-Kjær, G. De Filippo, H. Leth, S. Milosevic, A. Pahl, and J. O. P. Pedersen, in *28th EGAS Conference, Graz, Austria, 1996*, edited by L. Windholz, Europhysics Conference Abstracts Vol. 20D (European Physical Society, Mulhouse, France, 1996), pp. 240–241.